Detailed investigations on radiative opacity and emissivity of tin plasmas in the extreme-ultraviolet region

Jiaolong Zeng, Cheng Gao, and Jianmin Yuan

Department of Physics, College of Science, National University of Defense Technology, Changsha 410073, Hunan, People's Republic of China

Radiative opacity and emissivity of tin plasmas at average ionization degree of about 10 was investigated in detail by using a fully relativistic detailed level accounting approach, in which main physical effects on the opacity were carefully taken into account. Among these physical effects, configuration interaction, in particular core-valence electron correlations, plays an important role on the determination of accurate atomic data required in the calculation of opacity. It results in a strong narrowing of lines from all transition arrays and strong absorption is located in a narrow wavelength region of 12.5–14 nm for Sn plasmas. Using a complete accurate atomic data, we investigated the opacity of Sn plasmas at a variety of physical condition. Among the respective ions of Xe^{6+}-Xe^{15+}, Xe^{10+} has the largest absorption cross section at 13.5 nm, while the favorable physical condition for maximal absorption at 13.5 nm do not mean that Xe^{10+} has the largest fraction. Comparison with other theoretical results showed that a complete set of consistent accurate atomic data, which lacks very much, is essential to predict accurate opacity. Our atomic model is useful and can be applied to interpret opacity experiments. Further benchmark experiments are urgently needed to clarify the physical effects on the opacity of Sn plasmas.

I. INTRODUCTION

The search for optimum radiation source of emission with 2% wavelength bandwidth near 13.5 nm is important for the development of extreme ultraviolet radiation (EUV) lithography in the microelectronics industry [1]. Such an EUV lithography system requires an efficient light source with an average output of more than 115 W in a band of ±10% around 13.5 nm at the intermediate focus [2]. Tin is considered as a most promising target material for an efficient EUV source because of its high in-band conversion efficiency (CE) at 13.5 nm, which is attributed to $4d$-$4f$ and $4p$-$4d$ transitions of ion charge states of Sn^{7+}-Xe^{12+} in plasmas [3]. In order to improve the CE at 13.5 nm, various methods and techniques were developed in the experiments [4,5] including optimizing plasma condition of density and temperature for maximum efficiency [6,7] and by using doped targets or cavity targets [8,9].

For Sn^{7+}-Xe^{13+} ions, however, it is still a challenging work to obtain a complete set of accurate atomic data for the calculation of radiative property because of their complex atomic structure. They have a ground configuration of $4d^m$, where m is the occupation number of the $4d$ orbital. The collapse of $4d$, or even $4p$ and $4f$ orbital results in strong correlation effects among multielectrons of atomic ions. Furthermore, relativistic effects play an important role on their electronic structure. The configuration interaction (CI) effects and the relativistic effects are no more addictive in accurately treating the many electron systems, both of which must be considered simultaneously. Extensive efforts to produce more accurate atomic data for the investigation of radiation transport were carried out by a number of authors [10–15]. Dortan [10] theoretically investigated the influence of CI on satellite lines of Sn^{4+}-Xe^{13+} in the EUV region by using HULLAC parametric multiconfiguration relativistic code

[16]. Sasaki *et al.* [11,12] developed a collisional radiative model of tin plasmas to study the emissivity and opacity for the use of radiation hydrodynamics simulation. The atomic data required were obtained in the detailed configuration accounting (DCA) approximation. Koike and Fritzsche [13] discussed extensively the relativistic effects and electron correlation effects of tin ions by using the multiconfiguration Dirac Fock method. Kagawa *et al.* [14] carried out relativistic configuration interaction calculations for EUV spectra of Sn^{10+}-Xe^{12+} ions which are assumed to be embedded in a local thermodynamic equilibrium (LTE) plasma at a temperature of 30 eV. Karazija *et al.* [15] investigated the emission spectrum important for EUV lithography using the integral characteristics such as average energy, total line strength, variance and interval of transition array $4p^5 4d^{m+1} + 4p^5 4d^{m-1} 4f \rightarrow 4p^6 4d^m$. These theoretical researches are quite important for understanding the EUV physics, identifying emission lines and interpreting relevant experiments [17–22].

The parameters of Sn plasmas are of basic importance in understanding the physics of EUV light generation and transport and to benchmark the radiation hydrodynamic simulation codes in optimizing EUV sources. For optically thick Sn plasma at 13.5 nm, the EUV output is determined not only by the emissivity but also by the opacity of plasmas. However, there are few accurate investigations on the radiative opacity of Sn plasmas around ionization stage of Sn^{10+}. Most of the theoretical researches mentioned above treated accurately the main lines of $4p^5 4d^{m+1} + 4p^5 4d^{m-1} 4f \rightarrow 4p^6 4d^m$ by introducing electron correlations of $4d^2 - 4f^2$ and $4p^2 - 4d^2$ excitation. For $4d \rightarrow 4f$ and $4p \rightarrow 4d$ transitions from levels of excited configurations, however, electron correlations of $4d^2 - 4f^2$ and $4p^2 - 4d^2$ are not adequately taken into account. In order to obtain accurate radiative opacity, accurate atomic data are required not only for levels of ground configuration,

but also for levels of excited configurations. All of them should be based on the same footing. The opacity of Sn plasmas in the dominant EUV emission region is a critical parameter for investigating the optimum conditions for EUV generation. However, accurate opacity which can reliably be used for the design of EUV light source are short of very much in the literature. Lysaght *et al.* [23] measured the relative photoionization cross sections of neutral atom through Sn^{3+}. Fujioka *et al.* [24] experimentally measured an absorption spectrum of a uniform Sn plasma generated by thermal x rays in the wavelength region of 9–19 nm and investigated the opacity effects on the EUV emission. The average temperature and density of the heated Sn sample of 30 eV and 0.01 g/cm^3 at 1 ns after the peak of heating x-ray pulse. In order to better understand the physics of EUV radiative properties of Sn plasmas, there is an urgent need to obtain accurate opacity. In this work, we investigated the radiative opacity of Sn plasmas by using a complete and consistent set of accurate atomic data.

II. THEORETICAL METHOD

The detailed theoretical method for a detailed level accounting (DLA) scheme can be found elsewhere [25,26] and here only an outline is given. For an LTE plasma of temperature T and mass density ρ, the radiative opacity at radiation of energy $h\nu$ (h is the Planck constant and ν is the frequency of radiation) is given by

$$\rho\kappa'(h\nu) = [\mu_{bb}(h\nu) + \mu_{bf}(h\nu) + \mu_{ff}(h\nu)](1 - e^{-h\nu/kT}) + \mu_{scatt}(h\nu), \quad (1)$$

where μ_{bb}, μ_{bf}, μ_{ff}, and μ_{scatt} are absorption coefficients contributed by bound-bound, bound-free, free-free and scattering processes, respectively. The prime on the opacity denotes that stimulated emission has been taken into account.

In this work, we are mainly concerned with the opacity contributed by bound-bound transitions due to 4d-4f and 4p-4d around 13.5 nm. The bound-bound absorption coefficient can be obtained from the summation over all required bound-bound transition lines of all existing ionization stages in the plasmas,

$$\mu_{bb}(h\nu) = \sum_i \left(\sum_{ll'} N_{il}\sigma_{ill'}(h\nu) \right), \quad (2)$$

where N_{il} is population of the level l for ionization stage i and $\sigma_{ill'}(h\nu)$ is photoexcitation cross section from level l to l', which can be expressed in terms of the absorption oscillator strength $f_{ill'}$ as

$$\sigma_{ill'}(h\nu) = \frac{\pi h e^2}{m_e c} f_{ill'} S(h\nu), \quad (3)$$

where e and m_e are the electron charge and electron rest mass, respectively, c is the speed of light in vacuum, and S is the line shape function, which is taken as a Voigt profile, where line widths contributed by the Doppler and electron impact broadening mechanisms are included. The fraction of different charge states is determined by ionization equilib-

rium equation in LTE. The ionization potential depression is considered by using the Debye-Huckel model [27].

The fraction of radiation transmitted with respect to some incident source of arbitrary intensity is given by

$$F(h\nu) = e^{-\rho\kappa'(h\nu)L}. \quad (4)$$

where L is the path length traversed by the light source through the plasma. To compare directly with experiment, one should include the effects of instrumental broadening.

III. RESULTS AND DISCUSSION

The accuracy of opacity depends on the accuracy of the atomic data including the energy levels, oscillator strengths, photoionization cross sections and line widths caused by all kinds of broadening mechanisms. As mentioned in the above, one must treat simultaneously the CI and relativistic effects in a consistent way to obtain a complete set of accurate atomic data. For the effects of CI, one has to evaluate the inner-shell electron correlations precisely for all excited states as well as the ground state required in the calculation of opacity. Multiconfiguration Dirac-Fock (MCDF) code GRASP [28] was used for this purpose. In the MCDF method, an atomic state is approximated by a linear combination of configuration state functions (CSFs) of the same symmetry

$$\Phi_\alpha(J\pi) = \sum_i^{n_c} a_i(\alpha)|\gamma_i J\pi\rangle, \quad (5)$$

where n_c is the number of CSFs and $a_i(\alpha)$ denotes the representation of the atomic state in this basis. The CSFs are antisymmetrized products of a common set of orthonormal orbitals which are optimized on the basis of Dirac-Coulomb Hamiltonian. Further relativistic contributions to the atomic states due to Breit interactions are added by diagonalizing the Dirac-Coulomb-Breit Hamiltonian matrix. The dominant quantum electrodynamic contributions have also been included as a perturbation.

We take Sn^{10+} as an example to illustrate the combined effects of CI and relativity. The orbital wave functions are obtained by using an extended average level (EAL) method. The wave functions of Sn^{10+} are described by following one-electron relativistic orbitals: $1s_{1/2}$, $2s_{1/2}$, $2p_{1/2}$, $2p_{3/2}$, $3s_{1/2}$, $3p_{1/2}$, $3p_{3/2}$, $3d_{3/2}$, $3d_{5/2}$, $4s_{1/2}$, $4p_{1/2}$, $4p_{3/2}$, $4d_{3/2}$, $4d_{5/2}$, $4f_{5/2}$, $4f_{7/2}$, $5s_{1/2}$, $5p_{1/2}$, $5p_{3/2}$, $5d_{3/2}$, $5d_{5/2}$, $5f_{5/2}$, $5f_{7/2}$, $5g_{7/2}$, $5g_{9/2}$, $6s_{1/2}$, $6p_{1/2}$, $6p_{3/2}$, $6d_{3/2}$, and $6d_{5/2}$. The wave functions of the first 13 orbitals were obtained by optimizing the average energy of the ground configuration of $4s^24p^64d^4$, where the Ni-like core was omitted. Other orbitals were obtained by separate optimizations corresponding to the levels with different total angular momentum and parity. To take adequate CI into account and make the calculation tractable, we included the following configurations: $4s^24p^64d^4$, $4s^24p^64d^3nl$, $4s^24p^64d^24f^2$, $4s^24p^64d^24fnl$, $4s^24p^64d^25s^2$, $4s^24p^64d^25snl$, $4s^24p^64d^25p^2$, $4s^24p^64d^25pnl$, $4s^24p^64d4f^3$, $4s^24p^64d4f^25s$, $4s^24p^54d^5$, $4s^24p^54d^4nl$, $4s^24p^54d^34f^2$, $4s^24p^54d^34f5s$, $4s^24p^54d^34f5p$, $4s^24p^54d^34f5d$, $4s^24p^44d^6$, $4s^24p^44d^5nl$, $4s^24p^34d^7$, $4s4p^64d^5$, $4s4p^64d^45s$, $4s4p^64d^45p$, $4s4p^64d^45d$,
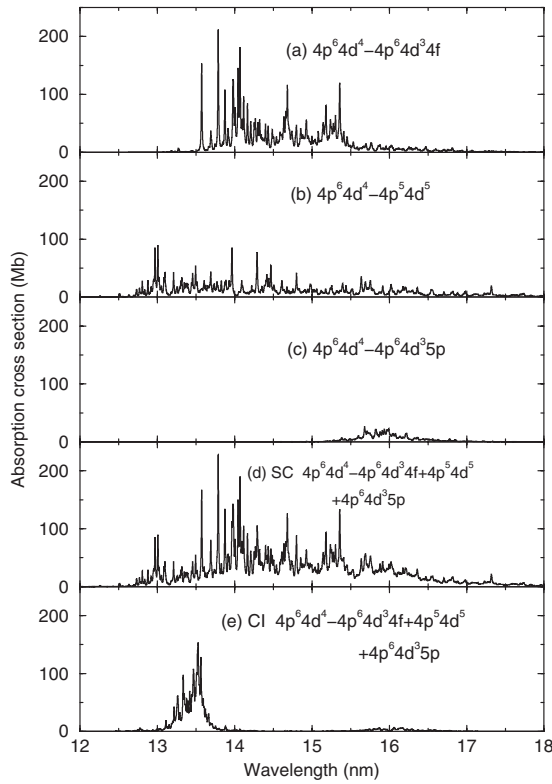
FIG. 1. Absorption cross section caused by transition arrays of (a) $4p^64d^4 \rightarrow 4p^64d^34f$, (b) $4p^64d^4 \rightarrow 4p^54d^5$, (c) $4p^64d^4 \rightarrow 4p^64d^35p$, and (d) the sum of these three transition arrays by using a single configuration Dirac-Fock calculation: (e) corresponds to a large-scale CI calculation of the same three transition arrays.

FIG. 2. (Color online) Spectrally resolved radiative opacity for Sn plasma at a temperature of 27 eV and a density of 0.01 g/cm^3 in a wavelength region of 8–18 nm: (a) total opacity (in a solid line) and (b) separate contributions of dominant ionization stages: The emissivity (in unit of 1 TW=1×10^{12} W) is given in a dotted red line.

where nl is restricted to the included orbitals. In this way, accurate atomic data can be obtained not only for the transition arrays from levels of the ground configuration, but also for the excited levels. From the list of configurations, one can see that $4d^2$-$4f^2$ and $4p^2$-$4d^2$ correlations are adequately included in the calculations. For more highly excited states which are not included in the above list yet their atomic data are needed in opacity calculation, these atomic data were obtained separately for every individual transition array one by one with electron correlations of $4d^2$-$4f^2$ and $4p^2$-$4d^2$ being taken into account.

The effects of CI on the oscillator strengths of Sn^{10+} can clearly be seen from Fig. 1, which shows the absorption cross section for the transition arrays of (a) $4s^24p^64d^4 \rightarrow 4s^24p^64d^34f$, (b) $4s^24p^64d^4 \rightarrow 4s^24p^54d^5$, and (c) $4s^24p^64d^4 \rightarrow 4s^24p^64d^35p$ of Sn^{10+}, respectively, by using single configuration (SC) calculations. Figures 1(d) and 1(e) show the summation of these three transition arrays by using SC and CI calculations, respectively. The relativistic effects have naturally included in all cases and therefore we will not discuss it separately hereafter. In order to obtain the results, Sn^{10+} was assumed to be embedded in an LTE tin plasma at a temperature of 27 eV and a density of 0.01 g/cm^3. From the comparison of the two plots of Figs. 1(d) and 1(e), one can see that a strong narrowing of lines from transitions of $4s^24p^64d^4 \rightarrow 4s^24p^64d^34f$ and $4s^24p^64d^4 \rightarrow 4s^24p^54d^5$ when complete CI was considered. The wavelength range of these

two transition arrays expanded from 12.5–18 nm for SC results, while it converged to a narrow region 13–14 nm with the strongest absorption being at a center of 13.5 nm. The increase or decrease of oscillator strengths with the CI are caused by the constructive-or destructive-interference effects in the radial portion of corresponding transition matrix. Mixing of basis functions owing to CI effect produces large changes in computing the oscillator strengths. For lines of transition array $4s^24p^64d^4 \rightarrow 4s^24p^64d^35p$, however, CI effects show different trend from the two strong transition arrays of $4s^24p^64d^4 \rightarrow 4s^24p^64d^34f$ and $4s^24p^64d^4 \rightarrow 4s^24p^54d^5$. Line position of $4s^24p^64d^4 \rightarrow 4s^24p^64d^35p$ was not greatly affected by CI effects, while the intensity is dramatically reduced. Similar phenomena apply to all transition arrays of all tin ions around Sn^{10+}. The redistribution of oscillator strengths between a transition array and between different arrays will surely have large effects on many practical applications of radiative atomic data, such as spectra analysis and radiative opacity calculation.

After investigating the CI effects on the oscillator strength of bound-bound transitions, in the following we showed CI effects on the opacity of Sn plasmas. Figure 2(a) shows the radiative opacity of LTE Sn plasma at a temperature of 27 eV and a density of 0.01 g/cm^3 in a solid line. The opacity shows strong absorption structures in a narrow region of 12–14 nm, beyond which the opacity is trivial. For LTE plasmas, the emissivity and opacity are related by Kirchhoff's law, and therefore it is easy to give the emissivity (in a dotted red line), which is defined by (at a given photon energy $h\nu$)
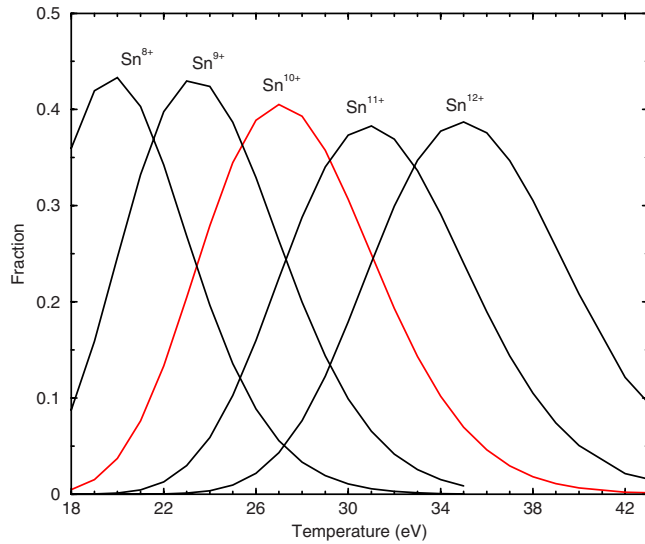
FIG. 3. (Color online) Fraction of Sn^{8+}-Sn^{12+} as a function of plasma temperature at a density of 0.01 g/cm^3.

$$\varepsilon_\nu = \sum_i \sum_{l<l'} h\nu N_{il'} A_{l'l} S_{l'l}(h\nu), \tag{6}$$

where $N_{il'}$ denotes the population of upper level l' of charge state i, $A_{l'l}$ is the spontaneous radiative transition probability for an emission line of $l' \rightarrow l$ and $S_{l'l}(h\nu)$ is the corresponding line profile function. As the wavelength of strong absorption is limited in a narrow region and therefore the structures shown in emissivity is similar to the opacity. As a result, the solid and dotted lines are nearly completely overlapped when proper scale is taken.

For tin plasma at the above physical condition, Sn^{8+}-Sn^{12+} have dominant contributions to the opacity. As far as the respective ion of Sn^{8+}-Sn^{12+}, the range of wavelength which they have the largest absorption is different. Figure 2(b) shows the opacity contributed by the respective ions. It can be seen that, at the wavelength of 13.5 nm, Sn^{10+} has the largest absorption although each ionization stage of Sn^{8+}-Sn^{12+} contributes to the opacity. In this figure, the population of each ionization stage has been taken into account. For Sn^{8+}-Sn^{12+}, the center of main lines $4d$-$4f$ and $4p$-$4d$ are located at about 14.1, 13.7, 13.5, 13.2, and 13.1 nm, respectively. If we eliminate the influence of populations on the opacity, we can know that Sn^{10+} has the largest absorption cross section at 13.5 nm. The satellite lines of Sn^{8+}, Sn^{9+}, Sn^{11+}, and Sn^{12+} have absorptions at 13.5 nm as well from the inspection of Fig. 2(b) and the absorption cross section for the respective ion is successively reduced with the increase of ionization stages from Sn^{8+} to Sn^{12+}. For plasmas in LTE, the emission intensity is proportional to the opacity, and therefore Sn^{10+} has the largest emission efficiency at 13.5 nm. We chose a density of 0.01 g/cm^3 which is a typical value of experimental access, at which density Sn^{10+} has the largest abundance at the temperature of 27 eV. Such a conclusion can easily be seen from Fig. 3, which shows the fraction of Sn^{8+}-Sn^{12+} as a function of temperature at a fixed density of 0.01 g/cm^3. From the above discussion, the ab-
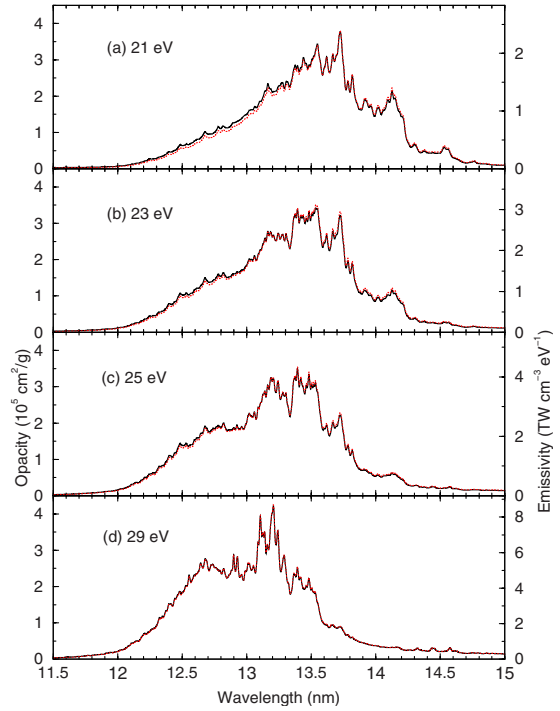
FIG. 4. (Color online) Spectrally resolved radiative opacity (solid lines) and emissivity (dotted red lines) for Sn plasma at temperatures of (a) 21 eV, (b) 23 eV, (c) 25 eV, and (d) 29 eV: the density is fixed to be 0.01 g/cm^3.

sorption or emission at 13.5 nm is a combined contribution from dominant ionization stages in the plasmas. The temperature of 27 eV does not necessarily correspond the strongest absorption at 13.5 nm. In order to see this, we show the opacity at different temperatures near 27 eV in Fig. 4 with the density being fixed to be 0.01 g/cm^3 in solid lines. It can be seen that the absorption at 13.5 nm is indeed a little stronger at temperatures of 23 and 25 eV than at 27 eV. On the other hand, the absorption is much weaker for plasmas at higher temperature of 29 eV at 13.5 nm. The emissivity is given for all cases as well. From the comparison of the different physical condition, one can see that the plasma at a temperature of 27 eV has the largest emissivity at the wavelength of 13.5 nm.

There are so many overlapping lines in the narrow region of 12–14 nm that the absorption around 13.5 nm constitutes a quasicontinuum region. Part of the reason for the coalesce of lines is due to the line width contributed by electron impact broadening. At the above density, the line width of spectral lines at 13.5 nm caused by Doppler broadening mechanism is about 0.0018 eV, while the typical line width caused by electron impact broadening is about 0.05 eV [29,30], and therefore, the latter is the main broadening mechanism. With the decrease of density, the line width contributed by electron impact broadening becomes smaller and the bound-bound line characteristics will be more evident, as illustrated in Fig. 5. It shows in a solid line the opacity at three different physical conditions: (a) 27 eV and 0.01 g/cm^3, (b) 22 eV and 0.001 g/cm^3, and (c) 18 eV and 0.0001 g/cm^3. The average ionization degree is about 10 for all three cases. The dashed lines show the contribution to the opacity of Sn^{10+}.
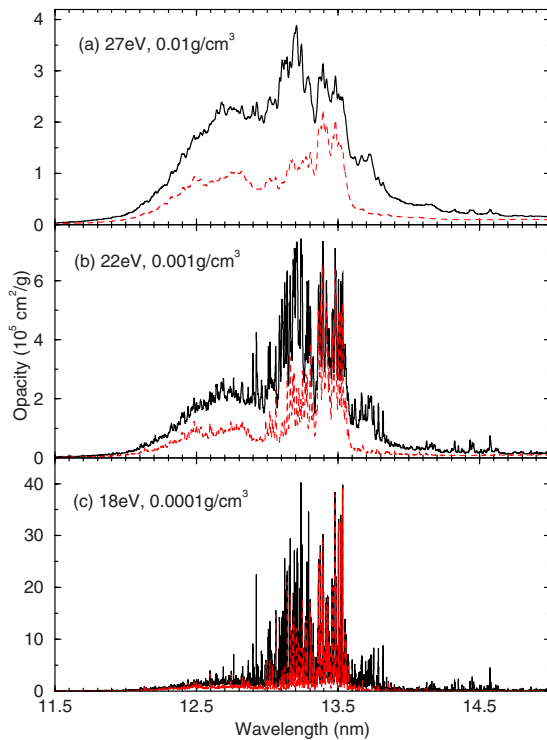
FIG. 5. (Color online) Spectrally resolved radiative opacity (solid lines) for Sn plasma at physical conditions of (a) 27 eV and 0.01 g/cm³, (b) 22 eV and 0.001 g/cm³, and (c) 18 eV and 0.0001 g/cm³: The dashed red lines represent the contributions of Sn¹⁰⁺.

In this work, great efforts were devoted to produce accurate atomic data and therefore the calculated opacity should be reliable. Yet theoretical modeling for the opacity of plasmas near ionization stage of Sn^{10+} is difficult and as a result there were few theoretical results published in the literature although there were so many opacity codes developed by researchers throughout the world. For experimental measurement, it is also a challenging work to create strict LTE condition for Sn plasmas. To the best of our knowledge, the only published experimental work on Sn plasmas was carried out by Fujioka *et al.* [24], yet preliminary analysis showed that Sn plasma deviated strongly from LTE condition. The average temperature and density of the heated Sn sample of 30 eV and 0.01 g/cm³ at 1 ns after the peak of heating x-ray pulse. The areal density of the Sn layer in the experiment was $2.04 \pm 0.18 \times 10^{-5}$ g/cm². Figure 6 shows the transmission of LTE Sn plasma at a mass density of 0.01 g/cm³ and temperatures of 20, 25, and 30 eV. The transmission was obtained from Eq. (4) and the required radiative opacity was calculated using the method described above. Another quantity of the path length L is assumed to be 2.04×10^{-3} cm, which was obtained from $\rho L = 2.04 \times 10^{-5}$ g/cm² with ρ being 0.01 g/cm³. For comparison, the raw and smoothed spectrum measured in the experiment of Fujioka *et al.* [24] were given in a dotted and dashed line. As reported by Fujioka *et al.* [24], the electron temperature and ion density of the dominant EUV emission region are in the ranges from 20 to 80 eV and from 10^{17} to 10^{20} cm⁻³, respectively, in the experiment. If the density of plasma is around 0.01 g/cm³,
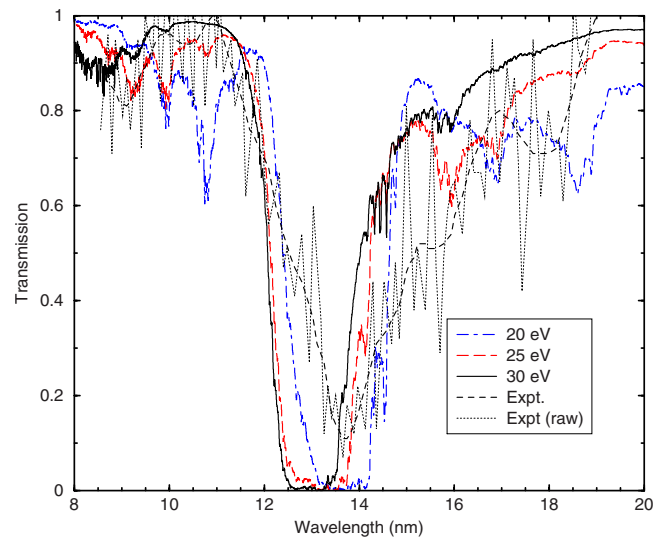
FIG. 6. (Color online) Comparison of our theoretical transmission with the experimental results carried out by Fujioka *et al.* [24].

the transmission will not show as evident line absorption structures as in the raw data, which can easily be seen from Fig. 5. The reason is that the line width caused by the physical broadening mechanisms such as electron impact broadening is large enough to fill the gaps between the lines. From the inspection of Fig. 6 for the raw experimental data, the mass density of the dominant EUV emission region shows evident information of much less than 0.01 g/cm³. The dominant ionization stages in the experimental plasma [24] were from Sn^{4+} to Sn^{15+}, resulting in a broader absorption range from 8–20 nm in the experimental transmission.
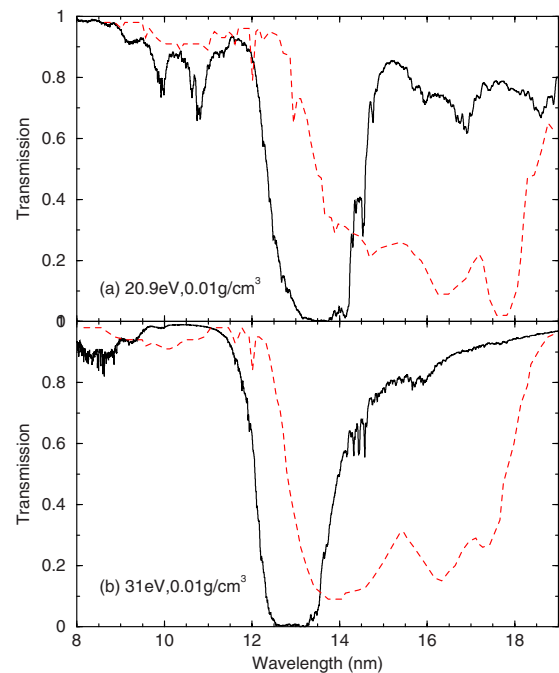
FIG. 7. (Color online) Comparison of our calculated transmission (solid lines) with theoretical results carried out by Fujioka *et al.* [24]: (dashed red lines) at temperature and density of (a) 20.9 eV and 0.01 g/cm³ and (b) 31 eV and 0.01 g/cm³, respectively.

To explain their experiment, Fujioka *et al.* [24] theoretically calculated the transmission of Sn plasmas. Figure 7 compares our theoretical results with their modeling by using the atomic code HULLAC [16] at the density of 0.01 g/cm^3 and electron temperatures of 20.9 and 31 eV, respectively. It can be seen that HULLAC predicted much broader absorption than ours and the predicted wavelength shifted toward higher wavelength direction. The most important reason is that Fujioka *et al.* [24] did not take adequate CI into account. As reported in their work, the authors included CI between the configurations of $4d^n$, $4d^{n-1}4f$, $4d^{n-1}5p$, $4d^{n-1}5f$, and $4p^54d^{n+1}$. As demonstrated in Fig. 1, correlations of two electron excitations such as $4d^2$-$4f^2$ and $4p^2$-$4d^2$ play an important role to obtained accurate atomic data.

In conclusion, spectrally resolved opacity and emissivity of Sn plasmas in EUV region centered at 13.5 nm were investigated in detail by using a complete set of accurate atomic data. A strong narrowing of lines from all transition arrays was found due to the effects of configuration interaction (including core-valence electron correlations) and very strong absorption is found only in a narrow wavelength region of 12.5–14 nm for Sn plasmas with the average ionization degree of about 10. Research showed that the main lines of $4d$-$4f$ and $4p$-$4d$ from the levels of ground configuration of Xe^{10+} are located near the center of 13.5 nm, while the main lines of nearby ions of Xe^{10+} deviate from the center of 13.5 nm. Near 13.5 nm only satellite lines from ionization stages around Xe^{10+} have absorptions, resulting in the largest absorption cross section of Xe^{10+} at 13.5 nm. Yet the favorable physical condition for maximal absorption at 13.5 nm do not mean that Xe^{10+} has the largest fraction. Comparison with other theoretical results showed that our calculated opacity predicted a much narrower absorption than others. In the strong absorption region of 12.5–14 nm, there are so many individual lines that statistical models should relatively easily give reasonable simulations for general characteristics, yet few such investigations were found in the literature. Further benchmark experiments are urgently needed to clarify the main physical effects on the opacity of Sn plasmas.

[1] G. Kubiak, L. Bernardez, and K. Krenz, Proc. SPIE **3331**, 81 (1998).

[2] U. Stamm, J. Phys. D: Appl. Phys. **37**, 3244 (2004).

[3] W. Svendsen and G. O'Sullivan, Phys. Rev. A **50**, 3710 (1994).

[4] T. Krucken, K. Bergmann, L. Juschkin, and R. Lebert, J. Phys. D: Appl. Phys. **37**, 3213 (2004).

[5] Y. Tao, M. S. Tillack, K. L. Sequoia, R. A. Burdt, S. Yuspeh, and F. Najmabadi, Appl. Phys. Lett. **92**, 251501 (2008).

[6] M. Masnavi, M. Nakajima, E. Hotta, and K. Horioka, J. Appl. Phys. **101**, 033306 (2007).

[7] Y. Tao, H. Nishimura, and S. Fujioka, Appl. Phys. Lett. **86**, 201501 (2005).

[8] S. S. Harilal, B. O'Shay, M. S. Tillack, Y. Tao, R. Paguio, A. Nikroo, and C. A. Back, J. Phys. D: Appl. Phys. **39**, 484 (2006).

[9] Y. Ueno, G. Soumagne, A. Sumitani, and A. Endo, Appl. Phys. Lett. **91**, 231501 (2007).

[10] F. de Gaufridy de Dortan, J. Phys. B **40**, 599 (2007).

[11] A. Sasaki, A. Sunahara, K. Nishihara, T. Nishikawa, K. Fujima, T. Kagawa, F. Koike, and H. Tanuma, High Energy Density Phys. **3**, 250 (2007).

[12] A. Sasaki, A. Sunahara, H. Furukawa, K. Nishihara, T. Nishikawa, F. Koike, and H. Tanuma, High Energy Density Phys. **5**, 147 (2009).

[13] F. Koike and S. Fritzsche, Radiat. Phys. Chem. **76**, 404 (2007).

[14] T. Kagawa, H. Tanuma, H. Ohashi, and K. Nishihara, J. Phys.: Conf. Ser. **58**, 149 (2007).

[15] R. Karazija, S. Kucas, and A. Momkauskaite, J. Phys. D: Appl. Phys. **39**, 2973 (2006).

[16] A. Bar-Shalom, J. Oreg, and M. Klapisch, Phys. Rev. E **56**, R70 (1997).

[17] R. D'Arcy, H. Ohashi, S. Suda, H. Tanuma, S. Fujioka, H. Nishimura, K. Nishihara, C. Suzuki, T. Kato, F. Koike, J. White, and G. O'Sullivan, Phys. Rev. A **79**, 042509 (2009).

[18] R. D'Arcy, H. Ohashi, S. Suda, H. Tanuma, S. Fujioka, H. Nishimura, K. Nishihara, C. Suzuki, T. Kato, F. Koike, A. O'Connor, and G. O'Sullivan, J. Phys. B **42**, 165207 (2009).

[19] E. R. Kieft, K. Garloff, J. J. A. M. van der Mullen, and V. Banine, Phys. Rev. E **71**, 036402 (2005).

[20] S. S. Churilov and A. N. Ryabtsev, Phys. Scr. **73**, 614 (2006).

[21] C. Suzuki, T. Kato, K. Sato, N. Tamura, D. Kato, S. Sudo, N. Yamamoto, H. Tanuma, H. Ohashi, S. Suda, and G. O'Sullivan, J. Phys.: Conf. Ser. **163**, 012019 (2009).

[22] H. Ohashi, S. Suda, H. Tanuma, S. Fujioka, H. Nishimura, K. Nishimura, T. Kai, A. Sasaki, N. Nakamura, and S. Ohtani, J. Phys.: Conf. Ser. **163**, 012071 (2009).

[23] M. Lysaght, D. Kilbane, N. Murphy, A. Cummings, P. Dunne, and G. O'Sullivan, Phys. Rev. A **72**, 014502 (2005).

[24] S. Fujioka *et al.*, Phys. Rev. Lett. **95**, 235004 (2005).

[25] J. Zeng, J. Yuan, and Q. Lu, Phys. Rev. E **64**, 066412 (2001).

[26] J. Zeng and J. Yuan, Phys. Rev. E **74**, 025401(R) (2006).

[27] D. J. Heading, J. S. Wark, G. R. Bennett, and R. W. Lee, J. Quant. Spectrosc. Radiat. Transf. **54**, 167 (1995).

[28] K. G. Dyall, I. P. Grant, C. T. Johnson, F. A. Parpia, and E. P. Plummer, Comput. Phys. Commun. **55**, 425 (1989).

[29] M. S. Dimitrijevic and N. Konjevic, J. Quant. Spectrosc. Radiat. Transf. **24**, 451 (1980).

[30] M. S. Dimitrijevic and N. Konjevic, Astron. Astrophys. **172**, 345 (1987).